Pseudonegative Thermal Expansion and the State of Water in Graphene Oxide Layered Assemblies

Jian Zhu,[†] Christine M. Andres,[†] Jiadi Xu,[‡] Ayyalusamy Ramamoorthy,[‡] Thomas Tsotsis,[§] and Nicholas A. Kotov[†,⊥,∥,*]

[†]Department of Chemical Engineering, University of Michigan, Ann Arbor 48109, United States, [‡]Department of Chemistry, University of Michigan, Ann Arbor 48109, United States, [§]The Boeing Company, Huntington Beach, California, United States, [⊥]Department of Materials Science and Engineering, University of Michigan, Ann Arbor 48109, United States, and [∥]Department of Biomedical Engineering, University of Michigan, Ann Arbor 48109, United States

ABSTRACT

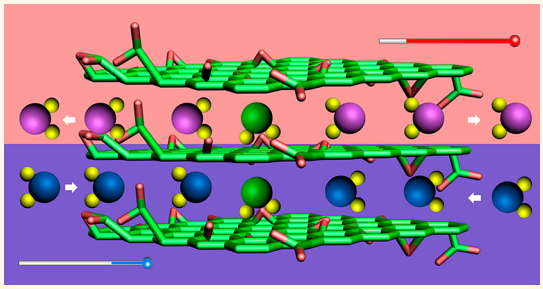

Unraveling the complex interplay between thermal properties and hydration is a part of understanding the fundamental properties of many soft materials and very essential for many applications. Here we show that graphene oxide (GO) demonstrates a highly negative thermal expansion (NTE) coefficient owing to unique thermohydration processes related with fast transport of water between the GO sheets, the amphiphilic nature of nanochannels, and close-to-zero intrinsic thermal expansion of GO. The humidity-dependent NTE of GO layered assemblies, or "pseudonegative thermal expansion" (PNTE), differs from that of other hygroscopic materials due to its relatively fast and highly reversible expansion/contraction cycles and occurrence at low humidity levels while bearing similarities to classic NTE. Thermal expansion of polyvinyl alcohol/GO composites is easily tunable with additional intricacy of thermohydration effects. PNTE combined with isotropy, nontoxicity, and mechanical robustness is an asset for applications of actuators, sensors, MEMS devices, and memory materials and crucial for developing methods of thermal/photopatterning of GO devices.

KEYWORDS: graphene oxide · GO · negative thermal expansion · layered · water adsorption · coefficient of thermal expansion · CTE

Typically materials expand on heating and have a positive coefficient of thermal expansion (CTE). The material expansion is associated with the general asymmetry of interatomic potential when the energy penalty for bringing bonded atoms closer together is steeper than for pulling them apart.[1] In some solids, however, other factors, such as phase transitions,[2] electronic valence transitions,[3] magnetorestiction,[4] transverse vibrations,[5,6] or topology,[7,8] may yield overall contraction at higher temperature, resulting in a phenomenon of negative thermal expansion (NTE). Such NTE materials are fundamentally interesting; however, their applications especially in zero-CTE composites[3,8] are limited due to poor scalability and toxicity (for instance, metal oxide- and cyanide-framework materials).[2,5,6] Also, the NTE effects are often very small and anisotropic as in Kevlar,[9] polyethylene fibers,[10] and carbon nanotubes,[11] showing a CTE below -5 ppm K^{-1}. Graphene was also found to display a negative yet small CTE of -6 or -8 ppm K^{-1} at 300 K[12,13] with a theoretically predicted value[14] of -3.8 ppm K^{-1}. Dense packing of graphene sheets reduces their out-of-plane deformation, and solid graphite shows an even smaller NTE of -1.5 ppm K^{-1} for 273–423 K.[15] Alternatively, a liquid crystal phase of nanographene with large intergallery spacing has shown a highly anisotropic NTE equal to -121, 91.2, and -59.6 ppm K^{-1} along the *a*, *b*, and *c* axes.[16] Large NTE materials with high mechanical properties are needed as a starting point for the preparation of zero-CTE composites,[3,8] actuators, sensors, and memory materials.

In this work we investigate the thermal behavior of graphene oxide (GO, Figure 1a), which demonstrates a highly negative apparent CTE associated with temperature-induced removal/insertion of interstitial water (thermohydration). The observed thermohydration effects can be described as pseudonegative thermal expansion (PNTE) and are more complex and surprising than might be expected from any previous studies.[17,18] As such, PNTE reveals a lot of similarities to classic NTE, exemplified by the reversibility of expansion–contraction cycles (Figure 1b) and retention of high

* Address correspondence to kotov@umich.edu.

Received for review July 12, 2012 and accepted August 3, 2012.

Published online August 03, 2012
10.1021/nn3031244

mechanical characteristics of the material (Figure S2c). Simultaneously, GO displays a number of unusual thermal expansion properties including the strong hysteresis of expansion/contraction rates. It is also quite surprising to see how low levels of humidity are needed for PNTE to take place. At present, the interplay between thermal properties and solvent/water incorporation cannot be easily predicted based on the current conceptual basis of soft matter and should be treated as a poorly understood property for such materials, with GO being just one of them. The recent findings about remarkable water permeation through GO[19] strongly indicate that there are potentially many unexpected phenomena related to water transport in GO and other materials.

The need for understanding the thermohydration effects is further underscored by many developing applications[17,20] in energy storage, MEMS, and actuators and is essential for the design of new memory materials. PNTE can be potentially useful for the rapidly evolving area of laser patterning of GO.[21,22] Importantly, while displaying large PNTE coefficients, GO is also associated with traits such as biocompatibility, scalability, and 2D isotropy, which are not shared by many other classic NTE materials.

RESULTS AND DISCUSSION

GO with a sheet thickness of 1 nm (Figure S1a) was prepared by the Hummers-Offeman method.[23] The layered GO assemblies (Figure 1a) were made through vacuum-assisted filtration, leading to *ca.* 18 μm thick free-standing film (GO paper),[17] or by spraying to obtain a GO coating with a thickness of *ca.* 100 nm.[19] Thermal expansion of a free-standing GO paper was studied by thermal mechanical analyzer (TMA). The TMA can eliminate grips-related errors, which can hardly be circumvented by other tools used in previous studies.[17,24] It is found that the length of GO paper shows reversible contraction/expansion upon heating/cooling (Figure 1b). Considering the facts that (1) the samples were exhaustively dried under vacuum for at least 48 h prior to the measurements; (2) exceptional care was taken to control the humidity of the sample environment including using ultrapure helium (99.9995%) as purging gas, and (3) a temperature window between 30 and 80 °C was purposefully selected to avoid any temperature-induced chemical changes in GO (see SI), the NTE of GO is initially attributed to deformation of the out-of-plane bonds (*i.e.*, the well-known membrane effect[25]). The dominance of out-of-plane over in-plane vibrational modes is hypothesized to significantly enhance the similar effects in graphene,[16] which can be a plausible NTE mechanism for GO. However, the exhaustive evaluation of the data reveals inconsistencies of this seemingly realistic hypothesis.[24] As such, if NTE occurs due to the out-of-plane deformation of bonds, this effect should be visible in NMR,[26] Raman, or FTIR[27]

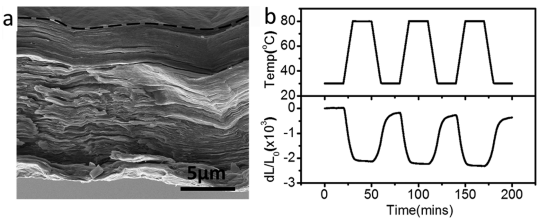

Figure 1. Properties of GO paper. (a) SEM image showing the cross-section of GO paper. (b) Thermal behavior of GO paper for repeated cooling and heating cycles at a relative humidity of 2.0% with the label d*L* standing for absolute length change and L_0 initial length at 30 °C.

spectroscopy, but the intensity and positions of the characteristic bands change insignificantly (Figure 2). In addition, the membrane effect would lead to a positive CTE in the direction transverse to the packing of GO sheets as a result of "bending" of the sheets. In contrast, the thermal behavior of GO paper still shows a negative expansion in this direction (Figure S5a).

We find that despite all the precautions and additional external isolation of the TMA probe in a specially made enclosure flooded with 99.9995% nitrogen, the continuous flux of ultrapure 99.9995% helium at 40 mL/min for as long as 24 h in the testing chamber cannot reduce the relative humidity to zero, related probably to the state of water in the sample and in the testing chamber. The humidity of the environment around the sample is found to depend on helium flow rate (Figure 3a−c), which becomes an important experimental parameter to consider. We also observe that the expansion of GO during the cooling stage continues after reaching the temperature plateau, *i.e.*, the isothermal stage at 30 °C. In contrast, the contraction of sample during the heating is virtually in sync with the temperature ramp. All these observations in aggregate indicate to us that thermohydration effects can potentially be the reason for apparent NTE behavior. For instance, the difference in expansion and contraction dynamics during cooling/heating ramps could be due to unequal rates of water adsorption/removal, which is in agreement with water sorption studies on freeze-dried food[28] and polyelectrolytes.[29,30] The difference is reduced when d*T*/d*t* is lowered from 5 °C/min to 1 °C/min without affecting the overall length changes as long as the humidity remains the same (Figure 3b *vs* 3c). In addition, since relative humidity is exponentially increased upon cooling (Figure S3a), an increase of length occurs with decreasing temperature before reaching a steady state.

The changes of sample length after long-term equilibration at a specific temperature (Figure S5b) are similar to those at faster temperature ramps, *i.e.*, 5 °C/min to 1 °C/min, and closely followed the *T*(*t*) trace (Figure 3c). This finding indicates the presence of an equilibrium state in the thermal trajectory, consistent with the thermodynamically reversible water adsorption/removal. Therefore, water-related thermal behavior of

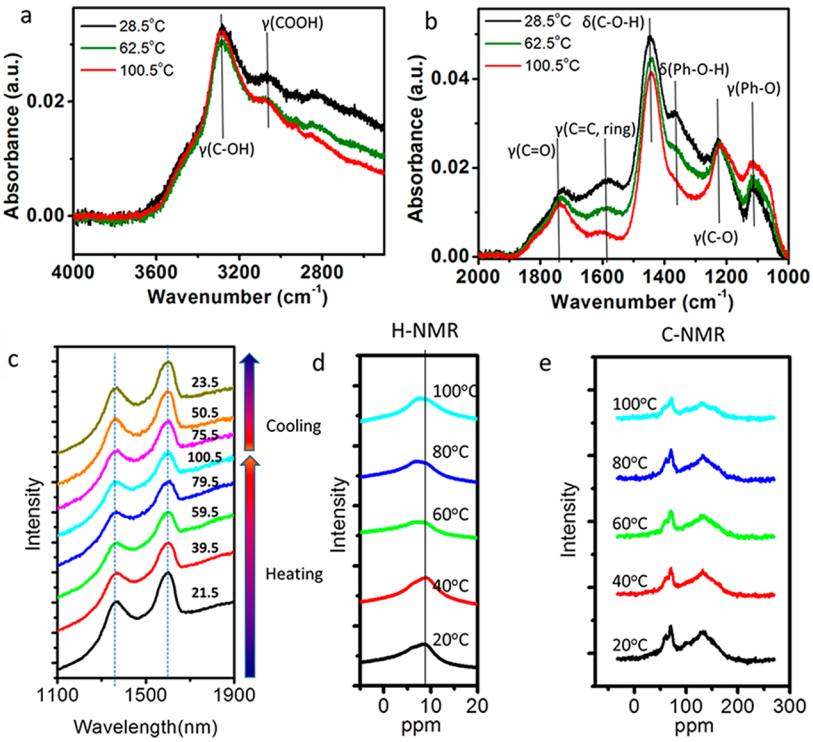

Figure 2. Thermal spectral analyses of GO paper. (a, b) *In situ* FTIR of GO sample at 28.5, 62.5, and 100.5 °C. The FTIR spectra[27] show vibration modes of various functional groups on the GO, including −OH stretching from C−OH (3289.1 cm^{-1}) and COOH (3094.8 cm^{-1}), C═O stretching (1736.1 cm^{-1}), aromatic ring (Ph) stretching (1610.3 cm^{-1}), −OH bending from COOH (1441.1 cm^{-1}) and Ph−OH (1368.8 cm^{-1}), and C−O stretching from Ph−O (1216.9 cm^{-1}) and C−O−C or C−OH (1109.4 cm^{-1}). All displayed FTIR spectral changes are reversible for cooling−heating cycles. (c) Raman spectra of GO at different temperatures. In the spectra, the D band (1368.8 cm^{-1}) and G band (1601.8 cm^{-1}) are shown. No significant shift was observed. (d) ^{1}H NMR and ^{13}C NMR spectra of GO at different temperatures. The peak in the ^{1}H NMR spectra mainly comes from C−OH and water. The ^{13}C NMR spectrum of GO consists of three resonance lines, at ca. 60, 70, and 130 ppm.[26] The first two peaks originate from tertiary C−OH and C−O−C groups, and the third is from the C═C bond.

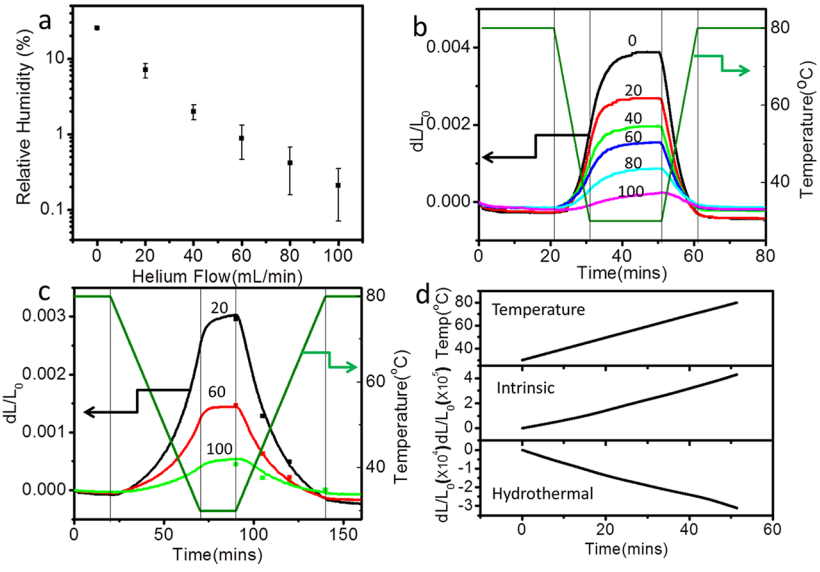

Figure 3. Thermal properties of thoroughly dried GO paper. (a) Dependence of the relative humidity of the TMA sample chamber on helium flow rates. (b and c) Thermal behaviors of GO paper at different relative humidity (helium flow rates) with temperature ramp rates of (b) 5 °C and (c) 1 °C/min. Solid points in (c) are in conditions of long-term equilibration at corresponding temperatures and relative humidity (helium flow rates). (d) Modulated thermal mechanical analysis of GO paper, showing temporal change of temperature, the changes of normalized length contributed by intrinsic (molecular) deformation and hydrothermal effect.

GO can be characterized by means of the CTE. Since thermal behavior is always nonlinear for GO, CTE is calculated by linearizing the data in a set of 10 °C intervals (Figure S4). As expected, CTE of GO is more negative at

higher humidity and less negative at higher temperatures. The most negative CTE values for 25%, 7.1%, 2.0%, 0.88%, 0.41%, and 0.21% humidity levels are −130.14, −94.17, −67.80, −51.4, −25.88, and −11.7 ppm K^{-1}, respectively (Figure S4). Notably, CTE values of GO are much larger in magnitude than those of reported NTE materials such as graphene,[12,13] carbon nanotubes,[11] Kevlar,[9] ZrW_2O_8,[5] $Zn(CN)_2$,[31] and $Cd(CN)_2$[31] even at a very low relative humidity of 0.21%.

Solid Materials with Large PNTE Associated with Thermohydration Effects Have Never Been Carefully Studied or Even Observed. Hydrogels (although not always solid materials) were reported to have irreversible shrinkage during drying.[32] Wood, a solid material with high equilibrium moisture content at high relative humidity, shows only −3 ppm K^{-1} at temperatures below 50 °C,[33] and its reversibility is questionable as a result of sorption hysteresis[34] attributed to changes in the complicated and irregular nanopore structures.[35] Other hygroscopic materials, such as cement paste,[36] show only positive CTE with a delayed response to temperature as a result of water transport. It can be argued that the presence of basal spacing between the GO sheets coupled with strong water uptake/desorption abilities leads to the manifestation of PNTE.

In order to study thermohydration effects in GO, powder X-ray diffraction (XRD) was applied (Figure 4a) to observe structural variations at room temperature under conditions allowing fast switching between "wet" and "dry" states. We changed the environment between (1) ambient air with a relative humidity of 35% and (2) an ultrapure nitrogen environment with untraceable humidity levels. In addition to the typical strong diffraction peaks within 2θ of 10−15°, which are usually assigned to stacks of hydrophilic regions with oxygenated functional groups on GO sheets, the sensitive XRD analyzer can also pick up weak signals for stacks of nonoxidized and hydrophobic graphitic regions in GO sheets (Figure 4c) with a typical spacing of 0.342 nm, which matches well with the 0.344 nm spacing of multilayer turbostratic graphene and is larger than the *d*-spacing of 0.335 nm in graphite.[37] The position of the weak "hydrophobic" peak is unaffected during the wet−dry switching, while the strong peak "hydrophilic" peak shifts almost immediately (<1 min) from 0.78 nm to 0.66 nm upon drying and quickly moves back at higher humidity (Figure 4b). Its intensity also increases from wet to dry state as a result of better ordering. Therefore water molecule can indeed be easily and reversibly inserted and removed from the GO layered assemblies in response to the humidity change. Due to close correlation between relative humidity and temperature (Figure S3a), this XRD experiment analysis also sheds light on what occurs in the material in response to temperature changes.

There are likely to be three types of water[38] in GO: "free water", which behaves like normal water without any confinement; "confined water", which encounters arbitrary constraints (GO sheets) while retaining translational mobility; and "bound water", which is tightly bound to GO by different bonds allowing only local motions. Standard Karl Fischer titration shows that "free water" and "confined water" in total constitute 21 wt % for a partially dried GO paper, while "bound water" constituted 8.8% of the sample (see Experimental Section). The "free water" can be completely removed from the GO sample by the vacuum drying, as evidenced by the absence of the corresponding peak in the DSC analysis (Figure S3b). Such water is certainly removed in the initial drying process in all the studies. As can be seen from XRD data in Figure 4, the GO water involved in PNTE is likely to be the "confined water". The "bound water" of GO cannot be removed without causing the irreversible reduction of the GO, but may be likely completely eliminated by drying the powdered GO.[39] The obtained anhydrous GO has a "hydrophilic" XRD peak of 0.57 nm,[39] which is obviously smaller than the 0.66 nm *d*-spacing after removing the "free" and "confined" water" in this study. Compared to the initial *d*-spacing of 0.78 nm, the change is 0.12 nm, which is much smaller than the van der Waals diameter of water, 0.282 nm.[40] Apparently, after the removal of water, the vacated space does not completely collapse, being supported by functional groups protruding in the basal spacing from the carbon grid. This unique structure makes a tremendous contribution to reversibility and the high rate of the diffusion process as the basal spaces vacated remain accessible and ready for the reinsertion of water molecules.

The process of adsorption and desorption of water molecules is further examined through NMR[26] and FTIR[27] spectroscopy (Figure 2a, b, d, and e). While features of the ^{13}C NMR spectra remain unchanged during the temperature sweep, ^{1}H NMR spectra (Figure 2d) show strong peak shifts from 9.1 ppm at 20−40 °C to 7.5 ppm at 40−100 °C, which are attributed to the loss of "confined water" (9.1 ppm), leaving behind the "bound water" (7.5 ppm) as the temperature increases.[41] In the FTIR spectra (Figure 2a), the intensity and position of O−H stretching mode are almost identical despite the desorption of water at higher temperatures, indicating that the hydrogen-bonding environment around the hydroxyl functional groups are barely disturbed due to the retained "bound water". The obvious change in the FTIR spectra is the weakening of the O−H bending mode from phenol (Ph−OH) at 1368.8 cm^{-1} at higher temperature, suggestive of the loss of hydrogen bonds with removed "confined water" molecules. Two points need to be made about this observation: (1) Inductive and resonance effects from phenyl rings lead to weaker hydrogen bonds between water and phenol groups, and therefore, these water molecules are easier to remove. (2) Phenyl rings are present at the edges of

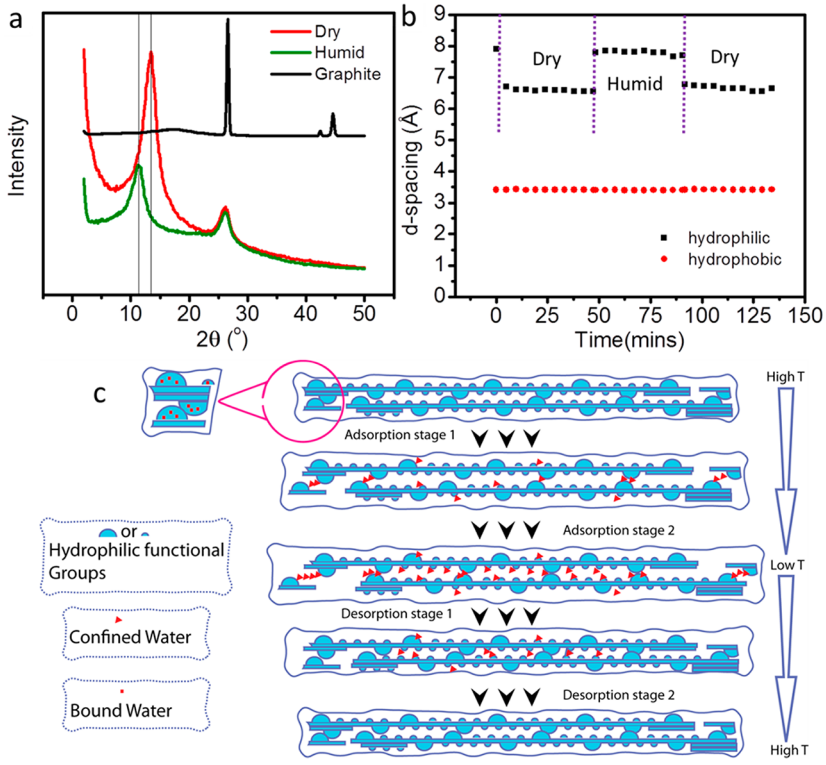

Figure 4. XRD analysis of GO paper. (a) Powder X-ray diffraction (XRD) pattern of GO paper for the dry and humid states. (b) Temporal trace of *d*-spacing for characteristic peaks in (a) with label "hydrophilic" for the peak of 2θ at 10−15° and "hydrophobic" for the peak at 2θ of 25−30°. (c) Schematic drawing of the water adsorption/desorption process in GO paper.

hydrophobic regions made of fused aromatic rings, which is one of the likely locations of the "confined water". The strongly "bound water" is instead localized at the most hydrophilic regions with multiple −COOH, −OH, and epoxy functional groups.

The temperature-induced process of water desorption is monitored by thermal gravimetrical analysis (TGA). At 22 °C, 9% of the weight is lost within 30 min in GO placed in a 100 mL/min flow of 99.9995% N_2. Fifty percent of the change occurs within 4 min, which is much longer than the period of <1 min for structure change/recovery in *in situ* XRD experiments (Figure 4). In addition, TMA analysis shows that 9−10 min is needed to reach a steady state (Figure 3b) upon cooling when water is readsorbed. Those results indicate that timing of the water desorption/adsorption process and the structural changes observed by XRD are markedly different. This finding and other experimental data can be explained by the model presented in Figure 4c. GO sheets are pillared by multiple islands constituted of protruding out-of-plane oxygenated functional groups and bound water between adjacent layers. In this case, the interlayer spacing is determined by islands from vertically adjacent sheets that touch each other. During the adsorption (cooling) stage, water molecules penetrate predominantly into the protruding islands in the hydrophilic regions, attach there, and lift the overall interlayer spacing. Here, GO in hydrophilic areas behaves as stiff nanoscale sheets, which correlates well with the data on their bending stiffness.[42] Fast saturation of these "elevated" hydrophilic regions gives fast shifts in the XRD 2θ peak in Figure 3 from 13.5° (0.66 nm) to 11.2° (0.78 nm). There are plenty of other areas on the GO sheets where water can be adsorbed. Then water saturates many other isolated islands and edges of the GO sheets. Concomitantly, GO sheets slide apart from each other due to water insertion, resulting in the increase of length of the GO paper. During this stage many islands that produced the shift in the "hydrophilic" XRD peak become misaligned, but the sheets remain supported by many other water "pillars". The desorption (heating) process reverses the structural changes but with the *d*-spacing collapsed more rapidly as a result of this misalignment and larger spacing. The interlayer spacing after that is 0.66 nm (Figure 4b), which is far larger than the van der Waals diameter of water, 0.282 nm,[40] allowing for completion of the desorption process and reversibility of the PNTE behavior.

The diffusivity of water in GO can be analytically described by the Crank equations.[43] Fitting the TGA curve at specific temperatures with the Crank equations yields the diffusion coefficient, D_{H2O}, of water in GO. At 22 °C it is estimated to be 8×10^{-14} m^2/s, and at 80 °C is 1.3×10^{-13} m^2/s (Figure 5a, b, c). This is larger than the diffusivity of water in some other hydrophilic polymers,[44] such as polyvinyl alcohol,[45] but smaller than in nylon and cellulose.[45] Note that D_{H2O} depends

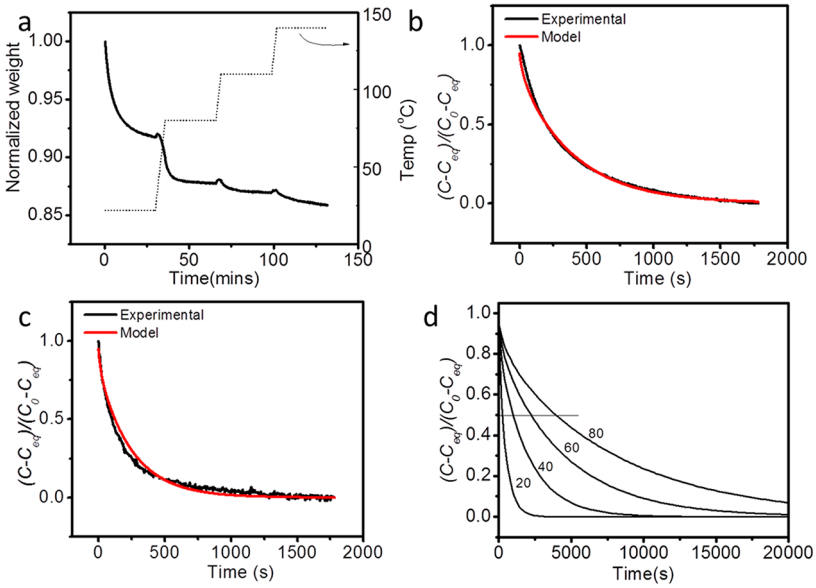

Figure 5. Water dynamic analyses in GO paper. (a) Water loss of GO measured by TGA. (b) The fitting of the Crank equation to the water loss data at 22 °C. (c) The fitting of the Crank equation to the water loss data at 80 °C. (d) Water diffusion prediction using the Crank equation for thicknesses of 20, 40, 60, and 80 μm at 22 °C.

on humidity. The ultrafast diffusion and permeation of water is observed when GO is exposed to water vapor,[19] while lower humidity results in much slower water diffusion. This result is not surprising and agrees with the model in Figure 4c: the narrowing of the 2D capillaries with the decreasing relative humidity blocks the flux of water,[19] and the diffusivity of water is impeded by the electrostatic drag exerted by protruding functional groups.

Knowing D_{H2O} allows us to analytically calculate the time scale of PNTE and compare it with the d*L*/*L* in curves in Figure 3b. Under the assumption that the thickness of the sample (18 μm) is much smaller than its width and length (2 × 15 mm), the calculated time to reach half-equilibrium is 4 min, which correlates fairly well with ca. 8 min found from Figure 3. The characteristic response time for thermohydration should increase with increasing thickness. Indeed, the characteristic time for 50% change quadruples when the thickness of GO doubles (Figure 5d).

A logical question then one can ask at this point is: "What is the intrinsic CTE (ICTE) of GO paper if one disregards thermohydration effects?" This question can be answered using state-of-the-art modulated temperature TMA, which uses a sinusoidal temperature profile (300 s period; amplitude ±5 °C) overlaid on a linear heating, cooling, or isothermal profile. In this way, one can separate thermal expansion by the characteristic time scale, which is much faster for intrinsic (molecular) CTE compared to PNTE. For fast cycling of temperature, water molecules are too slow to respond and can eliminate the contribution of hydrothermal effect to the thermal expansion under these modulated conditions, while the intrinsic expansion owing to vibrations of atoms in GO is in sync with the temperature modulations. The sample length change due to water removal is a magnitude higher than that from intrinsic thermal expansion. The magnitude of the overall change is similar to that in conventional TMA (100 mL/min helium flow rate, ramp rate of 1 °C/min, temperature window 30 to 80 °C). The average ICTE for the 30−80 °C range was 0.85 ppm (Figure 3d) and can be confirmed by the minimal changes of layer spacing at different temperatures in the ultrapure N_2 environment (Figure S6a). The very small ICTE of GO layered assemblies makes thermohydration effects more apparent. The ICTE of GO paper is also similar to the apparent CTE of chemically or thermally reduced graphene paper, which has a smaller number of hydrophilic groups in the nanochannels to interact with water molecules (Figure S6 b and c). Also note that the ICTE GO paper is positive and larger than that of graphite. This means that the larger basal spacing and crumpled morphology do not necessarily lead to more negative ICTE. The membrane effect causing NTE of graphene may be counteracted by hydrogen bonding and van der Waal forces holding the GO sheets together. Furthermore, the notion that the chemical groups protruding between the GO sheets are relatively free is erroneous; most of them are strongly confined by water molecules. The large NTE obtained for the crystal phase of nanographene assemblies[16] is due to the more accessible space in the gallery when the water adsorption is minimized. Clear confirmation and, in part, some of the same structural models of this model of thermohydration effects can be seen in the recent studies of water and solvent interactions with graphene oxide carried out by You *et al.*[54] and Talyzin *et al.*[55]

It is also possible to combine GO with other materials with positive CTE, resulting in a variety of composites being investigated for many applications.[46,47] Such materials can be excellent examples of the complexity of

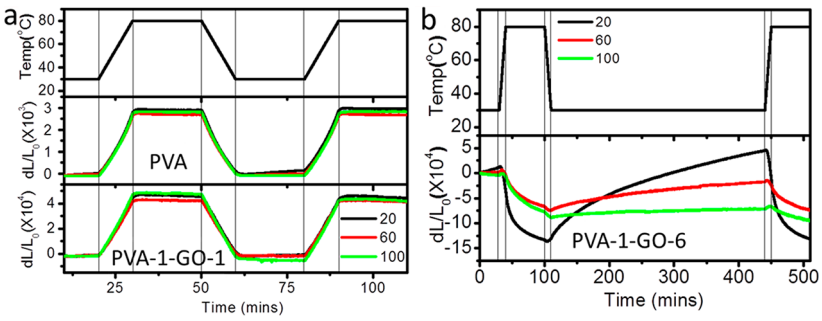

Figure 6. Thermal mechanical analysis of polyvinyl alcohol (PVA)/GO composites. Changes of dL/L_0 with temperature at different helium flow rates of 20, 60, and 100 mL/min for (a) PVA and PVA-1-GO-1 and (b) PVA-1-GO-6.

thermohydration effects. Polyvinyl alcohol (PVA)/GO composites were made by filtration after mixing PVA and GO at different ratios (Figure S7, Table S1). XRD analysis shows an increase of layer spacing after inclusion of PVA (Table S1), while neat PVA has an overall positive CTE of 56.8 ppm K^{-1} from 30 to 80 °C with a glass transition point at 70 °C (Figure 6a).[48] The incorporation of 81.1 wt % of GO into PVA (labeled as PVA-1-GO-1) reduces the CTE to 9.14 ppm K^{-1} (Figure 6b), which suggests GO sheets immobilize PVA chains. In addition, both PVA and PVA-1-GO-1 show perfect reversibility, no dependence on humidity, and no continuing deformation in the isothermal region despite being tested at a fast ramp rate of 5 °C/min. Further increase of GO content to 93.6 wt % (PVA-1-GO-6), however, does not result in reversible PNTE. Instead, PVA-1-GO-6 shows long saturation time during the isothermal stage and is highly influenced by the relative humidity. The instability and nonequilibrium nature of the expansion/contraction process make estimates of CTE ambiguous (Figure 6b). The slow equilibration rate indicates a slower diffusion process of water than that in the original GO layered assemblies. The inclusion of PVA leads to a more crowded space between GO sheets and higher drag exerted on diffusing water molecules. The diffusion completely stops for PVA-1-GO-1, making the CTE of the composite less dependent on relative humidity and more related with the ICTE of GO and PVA.

CONCLUSIONS

In summary, the fast water transport in response to the temperature and the close-to-zero intrinsic thermal expansion are responsible for PNTE in GO. The presence of multiple types of water and amphiphilic sites in GO makes its thermohydration behavior quite distinctive. The magnitude of PNTE displays obvious dependence on humidity, and so do the classic NTE materials. High mechanical strength, nontoxic nature, relative robustness, and variety of established methods for nanoscale materials engineering make PNTE materials an asset for a variety of applications.[49,50] Thermohydration effects in GO can also shed light on the fundamental issues in its use in charge storage, actuation, laser/heat patterning, and MEMS devices.

EXPERIMENTAL SECTION

Preparation of GO Paper and GO Coating. GO was prepared by the Hummers-Offeman method from graphite (Bay Carbon, SP-1).[17] Elemental analysis shows C:O:H = 43.26:53.41:3.33 in GO with 20.58 wt % mobile water and 8.76 wt % bound water included, which were determined by Karl Fischer titration when the sample was burned at 100 and 200 °C, respectively. GO dispersions (3 mg/mL) were prepared by sonication of GO in DI water for 30 min. GO paper was made by pouring the dispersion onto a 0.1 μm nylon filter under vacuum followed by thorough drying in a vacuum oven for 48 h.[17] GO coating was made by spraying a 0.5 mg/mL GO dispersion on a heated silicon surface at a temperature lower than 80 °C.

Preparation of Thermally and Chemically Reduced Graphene Paper. Thermally reduced graphene paper was prepared by heating the as-prepared GO paper at 300 °C for 1 h. In order to make chemically reduced graphene paper, 100 μL of hydrazine solution (50 wt %, Aldrich) and 700 μL of ammonia solution (28 wt %, Aldrich) were added into 200 mL of a 0.25 mg/mL GO dispersion, and the mixture was put into the 80 °C oven for 1 h.[51] The mixture was filtered through 0.1 μm nylon filter under vacuum to make chemically reduced graphene paper.

Coefficient of Thermal Expansion Measurement. (1) In-plane CTE measurement: The CTE of films was measured in extension mode by a Perkin-Elmer TMA7 following the ASTM test method for linear thermal expansion of solid materials by thermomechanical analysis (E 831) and slightly modified to measure thin films.[52,53] The extension probe and grips were customized by RT Instruments, Inc. to minimize the expansion of grips during the measurement (Figure S9). Ultrapure helium was used as purge gas to give an inert atmosphere and facilitate heat transfer. Cooling of the chamber was accomplished by circulating water at 8 °C provided by a chiller. The TMA instrument was calibrated using aluminum standard; the experimental error for CTE of aluminum was 7.6% for temperatures as high as 300 °C. The CTE of Kevlar fibers from DuPont was also measured as an additional calibration for negative expansion, yielding a value of −4.58 ppm K^{-1}, which agreed with the data reported in the literature.[9] GO paper strips that were 2 mm wide and 15 mm long were used for CTE measurements; the strips were stretched under 30 mN, and the length changes were recorded by monitoring probe displacement for temperature ramps of 5 and 1 °C/min. The sample was initially heated from 30 up to 80 °C and then stabilized for 2 h to remove free water and residual stress. The length change for both cooling and heating segments was used to calculate the CTE, represented by the slope of the curve normalized by the initial length at 30 °C. This parameter can be mathematically defined as CTE = $d(\Delta L/L_o)/dT$. The thermal curve was nonlinear; thus average CTEs

were calculated for every 10 °C interval. More than three samples were measured for each data point. (2) CTEs were also measured in the transversal (through-thickness) direction of GO assemblies. In order to achieve that, the thickness of the GO coating on silicon wafers was measured by a J.A. Woolham Co. VASE spectroscopic ellipsometer through fitting the Cauchy model with a homemade temperature-controlled stage. (3) Modulated temperature TMA was performed on GO paper samples by a Q400 thermomechanical analyzer in a lab of TA Instruments, Inc. The samples were cut into thin strips approximately 16 mm in length and 2.8 mm in width. Modulated TMA was used with an amplitude of ±5 °C, a period of 300 s, and a heating/cooling rate of 1 °C/min. The data from 30 to 80 °C in the second heating step were used in this paper.

Material Characterization. Element analysis and Karl Fischer titration were conducted by Galbraith Lab Inc. Differential scanning calorimetry (DSC) was carried out on a TA Instruments Q2000 DSC under a nitrogen atmosphere at a rate of 5 °C/min. The cross-section of the films was examined by FEI NOVA Nanolab scanning electron microscopy (SEM). ATR-FTIR spectroscopy was performed on a Nicolet 6700 spectrometer utilizing the grazing angle accessory (Smart SAGA) at a grazing angle of 85°. A drop of GO dispersion was put on a gold-coated silicon substrate and allowed to dry for 24 h. This sample was then attached onto a heat strip with temperature controller for *in situ* FTIR measurement. A similar setup was used for Raman measurement. Solid NMR experiments were performed on a 400 MHz NMR spectrometer with a spinning rate of 7 kHz on a 5 mm MAS probe. 1D ^{13}C NMR spectra were recorded using the Ramp CP pulse sequence with a CP time of 1 ms, and a decoupling of 70 kHz was applied. A 3 s recycle delay and 2048 scans were used for all experiments. Powder X-ray diffraction patterns of GO paper were collected at ambient temperature using a Rigaku R-AXIS SPIDER diffractometer with an imaging plate detector and graphite-monochromated Cu Kα radiation (1.5406 Å). Samples were glued to the tips of glass capillaries. Images were collected sequentially with a collection time of 2 min, and χ was set at 0° with the face of the film oriented parallel to the beam. Room-temperature ultrapure nitrogen (at 20 L/min) was controlled on and off to flow onto the sample. Images were integrated from 2.0° to 50° (2θ) with a 0.1° step size with the AreaMax (2.0.0.4 ed., Rigaku, 2005) software package. Powder patterns were processed in Jade 6.5 to calculate peak positions.

Conflict of Interest: The authors declare no competing financial interest.

Acknowledgment. The authors thank R. Ruoff from The University of Texas at Austin for the initial gift of GO dispersions and A. G. Wong-Foy and A. J. Matzger from University of Michigan for the XRD analysis of samples. This work is largely supported by AFOSR Mechanics of Multifunctional Materials & Microsystems Program grant FA9550-08-1-0382. This material is also based upon work partially supported by the Center for Solar and Thermal Energy Conversion, an Energy Frontier Research Center funded by the U.S. Department of Energy, Office of Science, Office of Basic Energy Sciences under Award Number #DE-SC0000957. This work was also supported in part by the Center for Photonic and Multiscale Nanomaterials (C-PHOM) funded by the National Science Foundation Materials Research Science and Engineering Center program DMR 1120923. We acknowledge as well the essential support from NSF under grant ECS-0601345; EFRI-BSBA 0938019; CBET 0933384; CBET 0932823; and CBET 1036672. Some instrumental measurements were made possible by AFOSR MURI 444286-P061716 and Army SBIR project A10-123. The authors thank the University of Michigan's EMAL for its assistance with electron microscopy, and for the NSF grant #DMR-9871177 for funding for the JEOL 2010F analytical electron microscope used in this work.

Supporting Information Available: Detailed analysis of the selection of temperature range for TMA testing, calculation of diffusion coefficient of water in GO paper, Table S1 for physical properties of various films tested in this study, and supporting Figures S1 to S9. This material is available free of charge *via* the Internet at http://pubs.acs.org.

Note Added after ASAP Publication: After the on-line publication of this paper on August 13, 2012, it came to our attention that we omitted highly relevant citations referring to the negative thermal expansion coefficient of graphene oxide and describing water-related phase transitions in graphite oxide. We apologize to the group of authors led by Prof. Talyzin for missing a citation of these publications which would be supportive of the suggested mechanism of pseudonegative thermal expansion. References 54 and 55 were added with corresponding citations in the text and the revised version was reposted on September 12, 2012.

REFERENCES AND NOTES

1. Evans, J. S. O. Negative Thermal Expansion Materials. *J. Chem. Soc., Dalton Trans.* **1999**, 3317–3326.
2. Rossetti, G. A.; Cline, J. P.; Navrotsky, A. Phase Transition Energetics and Thermodynamic Properties of Ferroelectric $PbTiO_3$. *J. Mater. Res.* **1998**, *13*, 3197–3206.
3. Salvador, J. R.; Guo, F.; Hogan, T.; Kanatzidis, M. G. Zero Thermal Expansion in Ybgage Due to an Electronic Valence Transition. *Nature* **2003**, *425*, 702–705.
4. Takenaka, K.; Takagi, H. Giant Negative Thermal Expansion in Ge-Doped Anti-Perovskite Manganese Nitrides. *Appl. Phys. Lett.* **2005**, *87*, 261902.
5. Mary, T. A.; Evans, J. S. O.; Vogt, T.; Sleight, A. W. Negative Thermal Expansion from 0.3 to 1050 K in ZrW_2O_8. *Science* **1996**, *272*, 90–92.
6. Goodwin, A. L.; Calleja, M.; Conterio, M. J.; Dove, M. T.; Evans, J. S. O.; Keen, D. A.; Peters, L.; Tucker, M. G. Colossal Positive and Negative Thermal Expansion in the Framework Material $Ag_3[Co(CN)_6]$. *Science* **2008**, *319*, 794–797.
7. Sigmund, O.; Torquato, S. Composites with Extremal Thermal Expansion Coefficients. *Appl. Phys. Lett.* **1996**, *69*, 3203.
8. Lakes, R. Cellular Solids with Tunable Positive or Negative Thermal Expansion of Unbounded Magnitude. *Appl. Phys. Lett.* **2007**, *90*, 221905.
9. Jain, A.; Vijayan, K. Kevlar 49 Fibres: Thermal Expansion Coefficients from High Temperature X-Ray Data. *Curr. Sci.* **2000**, *78*, 331–335.
10. Kobayash., Y; Keller, A. Temperature Coefficient of C Lattice Parameter of Polyethylene - an Example of Thermal Shrinkage Along Chain Direction. *Polymer* **1970**, *11*, 114–117.
11. Maniwa, Y.; Fujiwara, R.; Kira, H.; Tou, H.; Kataura, H.; Suzuki, S.; Achiba, Y.; Nishibori, E.; Takata, M.; Sakata, M.; Fujiwara, A.; Suematsu, H. Thermal Expansion of Single-Walled Carbon Nanotube (SWNT) Bundles: X-Ray Diffraction Studies. *Phys. Rev. B* **2001**, *64*, 241402.
12. Bao, W. Z.; Miao, F.; Chen, Z.; Zhang, H.; Jang, W. Y.; Dames, C.; Lau, C. N. Controlled Ripple Texturing of Suspended Graphene and Ultrathin Graphite Membranes. *Nat. Nanotechnol.* **2009**, *4*, 562–566.
13. Yoon, D.; Son, Y. W.; Cheong, H. Negative Thermal Expansion Coefficient of Graphene Measured by Raman Spectroscopy. *Nano Lett.* **2011**, *11*, 3227–3231.
14. Mounet, N.; Marzari, N. First-Principles Determination of the Structural, Vibrational and Thermodynamic Properties of Diamond, Graphite, and Derivatives. *Phys. Rev. B* **2005**, *71*, 205214.
15. Nelson, J. B.; Riley, D. P. The Thermal Expansion of Graphite from 15°C to 800°C. *Proc. Phys. Soc.* **1945**, *57*, 477–486.
16. Grigoriadis, C.; Haase, N.; Butt, H. J.; Mullen, K.; Floudas, G. Negative Thermal Expansion in Discotic Liquid Crystals of Nanographenes. *Adv. Mater.* **2010**, *22*, 1403–1406.
17. Dikin, D. A.; Stankovich, S.; Zimney, E. J.; Piner, R. D.; Dommett, G. H. B.; Evmenenko, G.; Nguyen, S. T.; Ruoff, R. S. Preparation and Characterization of Graphene Oxide Paper. *Nature* **2007**, *448*, 457–460.
18. Lerf, A.; Buchsteiner, A.; Pieper, J.; Schottl, S.; Dekany, I.; Szabo, T.; Boehm, H. P. Hydration Behavior and Dynamics of Water Molecules in Graphite Oxide. *J. Phys. Chem. Solids* **2006**, *67*, 1106–1110.
19. Nair, R. R.; Wu, H. A.; Jayaram, P. N.; Grigorieva, I. V.; Geim, A. K. Unimpeded Permeation of Water through Helium-Leak-Tight Graphene-Based Membranes. *Science* **2012**, *335*, 442–444.

20. Park, S.; Ruoff, R. S. Chemical Methods for the Production of Graphenes. *Nat. Nanotechnol.* **2009**, *4*, 217–224.
21. El-Kady, M. F.; Strong, V.; Dubin, S.; Kaner, R. B. Laser Scribing of High-Performance and Flexible Graphene-Based Electrochemical Capacitors. *Science* **2012**, *335*, 1326–1330.
22. Gao, W.; Singh, N.; Song, L.; Liu, Z.; Reddy, A. L. M.; Ci, L. J.; Vajtai, R.; Zhang, Q.; Wei, B. Q.; Ajayan, P. M. Direct Laser Writing of Micro-Supercapacitors on Hydrated Graphite Oxide Films. *Nat. Nanotechnol.* **2011**, *6*, 496–500.
23. Hummers, W. S.; Offeman, R. E. Preparation of Graphitic Oxide. *J. Am. Chem. Soc.* **1958**, *80*, 1339–1339.
24. Su, Y.; Wei, H.; Gao, R.; Yang, Z.; Zhang, J.; Zhong, Z.; Zhang, Y. Exceptional Negative Thermal Expansion and Viscoelastic Properties of Graphene Oxide Paper. *Carbon* **2012**, *50*, 2804–2809.
25. Lifshitz, I. Thermal Properties of Chain and Layered Structures at Low Temperatures. *Zh. Eksp. Teor. Fiz.* **1952**, *22*, 475–486.
26. He, H.; Riedl, T.; Lerf, A.; Klinowski, J. Solid-State NMR Studies of the Structure of Graphite Oxide. *J. Phys. Chem.* **1996**, *100*, 19954–19958.
27. Acik, M.; Lee, G.; Mattevi, C.; Chhowalla, M.; Cho, K.; Chabal, Y. J. Unusual Infrared-Absorption Mechanism in Thermally Reduced Graphene Oxide. *Nat. Mater.* **2010**, *9*, 840–845.
28. Saravacos, G. D.; Stinchfield, R. M. Effect of Temperature and Pressure on the Sorption of Water Vapor by Freeze-Dried Food Materials. *J. Food Sci.* **1965**, *30*, 779–786.
29. Ge, S.; Li, X.; Yi, B.; Hsing, I. M. Absorption, Desorption, and Transport of Water in Polymer Electrolyte Membranes for Fuel Cells. *J. Electrochem. Soc.* **2005**, *152*, A1149–A1157.
30. Tosto, S.; Knauth, P.; Di Vona, M. L. Water Adsorption/Desorption in Proton-Conducting Ionomer Membranes: The Model Case of Sulfonated and Silylated Poly-Ether-Ether-Ketone. *Solid State Ionics* **2012**, *209*, 9–14.
31. Goodwin, A. L.; Kepert, C. J. Negative Thermal Expansion and Low-Frequency Modes in Cyanide-Bridged Framework Materials. *Phys. Rev. B* **2005**, *71*, 140301.
32. Bar, A.; Ramon, O.; Cohen, Y.; Mizrahi, S. Shrinkage Behaviour of Hydrophobic Hydrogel during Dehydration. *J. Food Eng.* **2002**, *55*, 193–199.
33. Salmen, L. Thermal Expansion of Water Saturated Wood. *Holzforschung* **1990**, *44*, 17–19.
34. Glass, S. V.; Zelinka, S. L. *Wood Handbook*; U.S. Department of Agriculture, Forest Service: Madison, WI, 2010; Chapter 04: Moisture Relations and Physical Properties of Wood, pp 1—19.
35. Bazant, Z. P.; Bazant, M. Z. Theory of Soprtion Hysteresis in Nanoporous Solids: I. Snap-through Instablilities. *ArXiv preprint arXiv11084949* **2011**, 1−22.
36. Bazabt, Z. P. Delayed Thermal Dilatation of Cement Paste and Concrete Due to Mass Transport. *Nucl. Eng. Des.* **1970**, *14*, 308–318.
37. Li, Z. Q.; Lu, C. J.; Xia, Z. P.; Zhou, Y.; Luo, Z. X-Ray Diffraction Patterns of Graphite and Turbostratic Carbon. *Carbon* **2007**, *45*, 1686–1695.
38. Buchsteiner, A.; Lerf, A.; Pieper, J. Water Dynamics in Graphite Oxide Investigated with Neutron Scattering. *J. Phys. Chem. B* **2006**, *110*, 22328–22338.
39. Cerveny, S.; Barroso-Bujans, F.; Alegria, A.; Colmenero, J. Dynamics of Water Intercalated in Graphite Oxide. *J. Phys. Chem. C* **2010**, *114*, 2604–2612.
40. Franks, F. *Water: A Matrix of Life*; Royal Society of Chemistry: Cambridge, 2000; pp 43−44.
41. Lerf, A.; He, H.; Forster, M.; Klinowski, J. Structure of Graphite Oxide Revisited. *J. Phys. Chem. B* **1998**, *102*, 4477–4482.
42. Lee, C.; Wei, X. D.; Kysar, J. W.; Hone, J. Measurement of the Elastic Properties and Intrinsic Strength of Monolayer Graphene. *Science* **2008**, *321*, 385–388.
43. Crank, J. *The Mathematics of Diffusion*; Clarendon Press: Oxford, 1975; pp 1−414.
44. Marcovich, N. E.; Reboredo, M. M.; Aranguren, M. I. Moisture Diffusion in Polyester−Woodflour Composites. *Polymer* **1999**, *40*, 7313–7320.
45. Long, F. A.; Thompson, L. J. Diffusion of Water Vapor in Polymers. *J. Polym. Sci.* **1955**, *15*, 413–426.
46. Wang, S.; Tambraparni, M.; Qiu, J.; Tipton, J.; Dean, D. Thermal Expansion of Graphene Composites. *Macromolecules* **2009**, *42*, 5251–5255.
47. Balandin, A. A. Thermal Properties of Graphene and Nanostructured Carbon Materials. *Nat. Mater.* **2011**, *10*, 569–581.
48. Xu, J. Y.; Hu, Y.; Song, L.; Wang, Q. G.; Fan, W. C.; Liao, G. X.; Chen, Z. Y. Thermal Analysis of Poly(Vinyl Alcohol)/Graphite Oxide Intercalated Composites. *Polym. Degrad. Stab.* **2001**, *73*, 29–31.
49. Park, S.; An, J.; Suk, J. W.; Ruoff, R. S. Graphene-Based Actuators. *Small* **2010**, *6*, 210–212.
50. Ma, Y.; Zhang, Y.; Wu, B.; Sun, W.; Li, Z.; Sun, J. Polyelectrolyte Multilayer Films for Building Energetic Walking Devices. *Angew. Chem.* **2011**, *50*, 6254–6257.
51. Li, D.; Muller, M. B.; Gilje, S.; Kaner, R. B.; Wallace, G. G. Processable Aqueous Dispersions of Graphene Nanosheets. *Nat. Nanotechnol.* **2008**, *3*, 101–105.
52. Nogi, M.; Iwamoto, S.; Nakagaito, A. N.; Yano, H. Optically Transparent Nanofiber Paper. *Adv. Mater.* **2009**, *21*, 1595–1598.
53. Nishino, T.; Matsuda, I.; Hirao, K. All-Cellulose Composite. *Macromolecules* **2004**, *37*, 7683–7687.
54. You, S.; Luzan, S.; Yu, J.; Sundqvist, B.; Talyzin, A. V. Phase Transitions in Graphite Oxide Solvates at Temperatures Near Ambient. *J. Phys. Chem. Lett.* **2012**, *3*, 812–817.
55. Talyzin, A. V.; Luzan, S. M.; Szabo, T.; Chernyshev, D.; Dmitriev, V. Temperature dependent structural breathing of hydrated graphite oxide in H_2O. *Carbon* **2011**, *49*, 1894–1899.